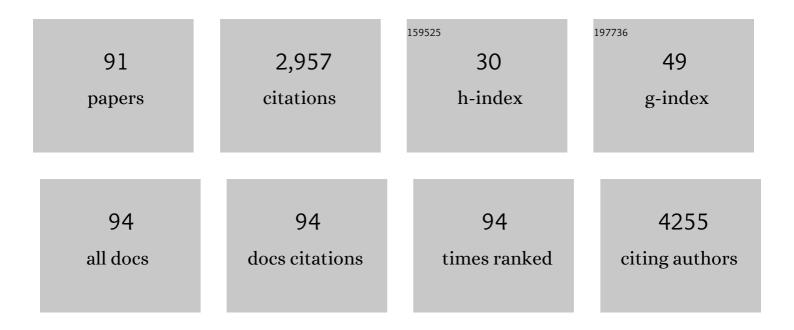
List of Publications by Year in descending order

Source: https://exaly.com/author-pdf/5516864/publications.pdf Version: 2024-02-01



CANC HUANC

#	Article	IF	CITATIONS
1	ImmunoPET imaging of hematological malignancies: From preclinical promise to clinical reality. Drug Discovery Today, 2022, 27, 1196-1203.	3.2	9
2	Annotating BCMA Expression in Multiple Myelomas. Molecular Pharmaceutics, 2022, 19, 3492-3501.	2.3	7
3	Annotating CD38 Expression in Multiple Myeloma with [¹⁸ F]F–Nb1053. Molecular Pharmaceutics, 2022, 19, 3502-3510.	2.3	10
4	RNA-binding protein p54nrb/NONO potentiates nuclear EGFR-mediated tumorigenesis of triple-negative breast cancer. Cell Death and Disease, 2022, 13, 42.	2.7	7
5	The Added Value of ¹⁸ F-FDG PET/CT Compared with ⁶⁸ Ga-PSMA PET/CT in Patients with Castration-Resistant Prostate Cancer. Journal of Nuclear Medicine, 2022, 63, 69-75.	2.8	26
6	GPC3-targeted immunoPET imaging of hepatocellular carcinomas. European Journal of Nuclear Medicine and Molecular Imaging, 2022, 49, 2682-2692.	3.3	23
7	Engineering nanobodies for next-generation molecular imaging. Drug Discovery Today, 2022, 27, 1622-1638.	3.2	16
8	Regulatory mechanism of α-hederin upon cisplatin sensibility in NSCLC at safe dose by destroying GSS/GSH/GPX2 axis–mediated glutathione oxidation-reduction system. Biomedicine and Pharmacotherapy, 2022, 150, 112927.	2.5	10
9	Molecular Imaging of Renal Cell Carcinoma in Precision Medicine. Molecular Pharmaceutics, 2022, 19, 3457-3470.	2.3	5
10	Shikonin inhibited glycolysis and sensitized cisplatin treatment in non-small cell lung cancer cells via the exosomal pyruvate kinase M2 pathway. Bioengineered, 2022, 13, 13906-13918.	1.4	25
11	Cisplatin-resistant NSCLC cells induced by hypoxia transmit resistance to sensitive cells through exosomal PKM2. Theranostics, 2021, 11, 2860-2875.	4.6	90
12	PD-L1 correlated gene expression profiles and tumor infiltrating lymphocytes in pancreatic cancer. International Journal of Medical Sciences, 2021, 18, 3150-3157.	1.1	2
13	ImmunoPET imaging of multiple myeloma with [68Ga]Ga-NOTA-Nb1053. European Journal of Nuclear Medicine and Molecular Imaging, 2021, 48, 2749-2760.	3.3	34
14	Diagnostic value of 18F-FDG PET/CT in patients with biochemical recurrent prostate cancer and negative 68Ga-PSMA PET/CT. European Journal of Nuclear Medicine and Molecular Imaging, 2021, 48, 2970-2977.	3.3	22
15	ImmunoPET imaging of human CD8+ T cells with novel 68Ga-labeled nanobody companion diagnostic agents. Journal of Nanobiotechnology, 2021, 19, 42.	4.2	30
16	The added value of ¹⁸ F-FDG PET/CT compared to ⁶⁸ Ga-PSMA PET/CT in patients with castration-resistant prostate cancer. Journal of Nuclear Medicine, 2021, , jnumed.121.262250.	2.8	7
17	CaCO ₃ â€Encapuslated Microspheres for Enhanced Transhepatic Arterial Embolization Treatment of Hepatocellular Carcinoma. Advanced Healthcare Materials, 2021, 10, e2100748.	3.9	15
18	Next-Generation Molecular Imaging of Thyroid Cancer. Cancers, 2021, 13, 3188.	1.7	6

#	Article	IF	CITATIONS
19	Nuclear scaffold protein p54nrb/NONO facilitates the hypoxia-enhanced progression of hepatocellular carcinoma. Oncogene, 2021, 40, 4167-4183.	2.6	12
20	Novel SREBP1 inhibitor cinobufotalin suppresses proliferation of hepatocellular carcinoma by targeting lipogenesis. European Journal of Pharmacology, 2021, 906, 174280.	1.7	18
21	LncRNA AC020978 facilitates non–small cell lung cancer progression by interacting with malate dehydrogenase 2 and activating the AKT pathway. Cancer Science, 2021, 112, 4501-4514.	1.7	12
22	Corosolic acid reduces A549 and PC9 cell proliferation, invasion, and chemoresistance in NSCLC via inducing mitochondrial and liposomal oxidative stress. Biomedicine and Pharmacotherapy, 2021, 144, 112313.	2.5	6
23	Advancing the diagnosis of epithelioid hemangioendothelioma by F-FDG PET/CT. American Journal of Nuclear Medicine and Molecular Imaging, 2021, 11, 230-232.	1.0	Ο
24	Synthesis and Evaluation of Ga-68-Labeled Rhein for Early Assessment of Treatment-Induced Tumor Necrosis. Molecular Imaging and Biology, 2020, 22, 515-525.	1.3	10
25	Noninvasive Classification of Human Triple Negative Breast Cancer by PET Imaging with GRP78-Targeted Molecular Probe [68Ga]DOTA-VAP. Molecular Imaging and Biology, 2020, 22, 772-779.	1.3	4
26	Prognostic Values of TIGAR Expression and ¹⁸ F-FDG PET/CT in Clear Cell Renal Cell Carcinoma. Journal of Cancer, 2020, 11, 1-8.	1.2	10
27	Predicting Therapeutic Efficacy of Vascular Disrupting Agent CA4P in Rats with Liver Tumors by Hepatobiliary Contrast Agent Mn-DPDP-Enhanced MRI. Translational Oncology, 2020, 13, 92-101.	1.7	11
28	HDAC8-dependent deacetylation of PKM2 directs nuclear localization and glycolysis to promote proliferation in hepatocellular carcinoma. Cell Death and Disease, 2020, 11, 1036.	2.7	25
29	Epigenetic Changes Associated With Interleukin-10. Frontiers in Immunology, 2020, 11, 1105.	2.2	21
30	ImmunoPET: Concept, Design, and Applications. Chemical Reviews, 2020, 120, 3787-3851.	23.0	263
31	Predicting EGFR mutation subtypes in lung adenocarcinoma using 18F-FDG PET/CT radiomic features. Translational Lung Cancer Research, 2020, 9, 549-562.	1.3	51
32	Proteoglycan 4 predicts tribological properties of repaired cartilage tissue. Theranostics, 2020, 10, 2538-2552.	4.6	4
33	Programming bulk enzyme heterojunctions for biosensor development with tetrahedral DNA framework. Nature Communications, 2020, 11, 838.	5.8	84
34	Hypoxia-induced IncRNA-AC020978 promotes proliferation and glycolytic metabolism of non-small cell lung cancer by regulating PKM2/HIF-11± axis. Theranostics, 2020, 10, 4762-4778.	4.6	151
35	Delayed ¹⁸ F FDG PET/CT Imaging in the Assessment of Residual Tumors after Transurethral Resection of Bladder Cancer. Radiology, 2019, 293, 144-150.	3.6	15
36	<p>Protein kinase C-iota-mediated glycolysis promotes non-small-cell lung cancer progression</p> . OncoTargets and Therapy, 2019, Volume 12, 5835-5848.	1.0	15

#	Article	IF	CITATIONS
37	LINC01123, a c-Myc-activated long non-coding RNA, promotes proliferation and aerobic glycolysis of non-small cell lung cancer through miR-199a-5p/c-Myc axis. Journal of Hematology and Oncology, 2019, 12, 91.	6.9	160
38	Upregulated circRNA ARHGAP10 Predicts an Unfavorable Prognosis in NSCLC through Regulation of the miR-150-5p/GLUT-1 Axis. Molecular Therapy - Nucleic Acids, 2019, 18, 219-231.	2.3	62
39	Relationship between the expression of PD-1/PD-L1 and 18F-FDG uptake in bladder cancer. European Journal of Nuclear Medicine and Molecular Imaging, 2019, 46, 848-854.	3.3	60
40	<scp>SIRT</scp> 5â€mediated deacetylation of <scp>LDHB</scp> promotes autophagy and tumorigenesis in colorectal cancer. Molecular Oncology, 2019, 13, 358-375.	2.1	92
41	Radioactive Iodine Therapy in Patients with Differentiated Thyroid Cancer: Study of External Dose Rate Attenuation Law and Individualized Patient Management. Thyroid, 2019, 29, 93-100.	2.4	4
42	18F-Deoxyglucose (18F-FDG) Positron Emission Tomography/Computed Tomography (PET/CT) Monitoring of Dynamic Growth Characteristics of Walker-256 Tumor Models in 3 Different Locations in Rats. Medical Science Monitor, 2019, 25, 558-564.	0.5	2
43	Pyruvate kinase M2 interacts with nuclear sterol regulatory element–binding protein 1a and thereby activates lipogenesis and cell proliferation in hepatocellular carcinoma. Journal of Biological Chemistry, 2018, 293, 6623-6634.	1.6	47
	Evaluation of the novel TSPO radiotracer		

#	Article	IF	CITATIONS
55	3D Segmentation of Residual Thyroid Tissue Using Constrained Region Growing and Voting Strategies. , 2017, , .		0
56	An Imaging and Histological Study on Intrahepatic Microvascular Passage of Contrast Materials in Rat Liver. BioMed Research International, 2017, 2017, 1-11.	0.9	1
57	A Computer-Aided Analysis Method of SPECT Brain Images for Quantitative Treatment Monitoring: Performance Evaluations and Clinical Applications. BioMed Research International, 2017, 2017, 1-11.	0.9	3
58	¹⁸ F-fluorodeoxyglucose uptake predicts MET expression in lung adenocarcinoma. OncoTargets and Therapy, 2017, Volume 10, 5643-5651.	1.0	0
59	Potential clinical value of PET/CT in predicting occult nodal metastasis in T1-T2NOMO lung cancer patients staged by PET/CT. Oncotarget, 2017, 8, 82437-82445.	0.8	14
60	Report on the development and application of PET/CT in mainland China. Oncotarget, 2017, 8, 64417-64426.	0.8	6
61	Micro-HCCs in rats with liver cirrhosis: paradoxical targeting effects with vascular disrupting agent CA4P. Oncotarget, 2017, 8, 55204-55215.	0.8	7
62	The Role of ¹⁸ F-FDG PET/CT and MRI in Assessing Pathological Complete Response to Neoadjuvant Chemotherapy in Patients with Breast Cancer: A Systematic Review and Meta-Analysis. BioMed Research International, 2016, 2016, 1-10.	0.9	32
63	Standardization of Administered Activities in Pediatric Nuclear Medicine: A Report of the First Nuclear Medicine Global Initiative Project, Part 2—Current Standards and the Path Toward Global Standardization. Journal of Nuclear Medicine, 2016, 57, 1148-1157.	2.8	26
64	⁶⁴ CuSâ€labeled nanoparticles: a new sentinelâ€lymphâ€nodeâ€mapping agent for PET–CT and photoacoustic tomography. Contrast Media and Molecular Imaging, 2016, 11, 475-481.	0.4	14
65	Cerebral blood perfusion changes in amputees with myoelectric hands after rehabilitation: a SPECT computer-aided analysis. BMC Neuroscience, 2016, 17, 59.	0.8	3
66	A multifunctional contrast dye for morphological research. Microscopy Research and Technique, 2016, 79, 111-121.	1.2	1
67	Fluorine-18-fluorodeoxyglucose positron emission tomography to evaluate recurrent gastric cancer after surgical resection: a systematic review and meta-analysis. Annals of Nuclear Medicine, 2016, 30, 179-187.	1.2	23
68	Arginine Methylation of SREBP1a via PRMT5 Promotes <i>De Novo</i> Lipogenesis and Tumor Growth. Cancer Research, 2016, 76, 1260-1272.	0.4	90
69	Relationship Between ¹⁸ F-FDG PET/CT Findings and HER2 Expression in Gastric Cancer. Journal of Nuclear Medicine, 2016, 57, 1040-1044.	2.8	52
70	miR-22 inhibits tumor growth and metastasis by targeting ATP citrate lyase: evidence in osteosarcoma, prostate cancer, cervical cancer and lung cancer. Oncotarget, 2016, 7, 44252-44265.	0.8	148
71	Inhibition of SREBP increases gefitinib sensitivity in non-small cell lung cancer cells. Oncotarget, 2016, 7, 52392-52403.	0.8	37
72	Prognostic value of total lesion glycolysis of baseline 18F-fluorodeoxyglucose positron emission tomography/computed tomography in diffuse large B-cell lymphoma. Oncotarget, 2016, 7, 83544-83553.	0.8	48

#	Article	IF	CITATIONS
73	Differential diagnosis of gallstones by using hypericin as a fluorescent optical imaging agent. World Journal of Gastroenterology, 2016, 22, 6690.	1.4	2
74	Prognostic significance of 18FDG PET/CT in colorectal cancer patients with liver metastases: a meta-analysis. Cancer Imaging, 2015, 15, 19.	1.2	64
75	Threeâ€dimensional contrasted visualization of pancreas in rats using clinical MRI and CT scanners. Contrast Media and Molecular Imaging, 2015, 10, 379-387.	0.4	11
76	Differentiation between Malignant and Benign Solitary Lesions in the Liver with ¹⁸ FDG PET/CT: Accuracy of Age-related Diagnostic Standard. Journal of Cancer, 2015, 6, 40-47.	1.2	6
77	Dichloroacetate restores drug sensitivity in paclitaxel-resistant cells by inducing citric acid accumulation. Molecular Cancer, 2015, 14, 63.	7.9	47
78	Standardization of Administered Activities in Pediatric Nuclear Medicine: A Report of the First Nuclear Medicine Global Initiative Project, Part 1—Statement of the Issue and a Review of Available Resources. Journal of Nuclear Medicine, 2015, 56, 646-651.	2.8	32
79	Mammalian models of chemically induced primary malignancies exploitable for imaging-based preclinical theragnostic research. Quantitative Imaging in Medicine and Surgery, 2015, 5, 708-29.	1.1	67
80	A Regulatory Feedback Loop between HIF-11 \pm and PIM2 in HepG2 Cells. PLoS ONE, 2014, 9, e88301.	1.1	22
81	HSP40 Interacts with Pyruvate Kinase M2 and Regulates Glycolysis and Cell Proliferation in Tumor Cells. PLoS ONE, 2014, 9, e92949.	1.1	31
82	Relationship Between ¹⁸ F-FDG Accumulation and Lactate Dehydrogenase A Expression in Lung Adenocarcinomas. Journal of Nuclear Medicine, 2014, 55, 1766-1771.	2.8	50
83	Lens culinaris agglutinin-reactive α-fetoprotein decline after transcatheter arterial chemoembolization in patients with hepatocellular carcinoma predicts survival. Clinica Chimica Acta, 2014, 431, 232-238.	0.5	13
84	Using a yeast two-hybrid system to identify FTCD as a new regulator for HIF-1α in HepG2 cells. Cellular Signalling, 2014, 26, 1560-1566.	1.7	16
85	SIRT1-Mediated Deacetylation of CRABPII Regulates Cellular Retinoic Acid Signaling and Modulates Embryonic Stem Cell Differentiation. Molecular Cell, 2014, 55, 843-855.	4.5	60
86	Dichloroacetate Enhances Adriamycin-Induced Hepatoma Cell Toxicity In Vitro and In Vivo by Increasing Reactive Oxygen Species Levels. PLoS ONE, 2014, 9, e92962.	1.1	31
87	Inhibition of SIRT6 in prostate cancer reduces cell viability and increases sensitivity to chemotherapeutics. Protein and Cell, 2013, 4, 702-710.	4.8	99
88	TIGAR Is Correlated with Maximal Standardized Uptake Value on FDG-PET and Survival in Non-Small Cell Lung Cancer. PLoS ONE, 2013, 8, e80576.	1.1	18
89	Inhibition of the overexpressing SIRT6 sensitizes prostate cancer cells to chemotherapeutics. FASEB Journal, 2012, 26, lb521.	0.2	0
90	Estimate of fibrosis in carbon tetrachloride induced chronic liver injury in rat by breath test with Lâ€{1â€13C] phenylalanine. FASEB Journal, 2009, 23, 741.10.	0.2	0

#	Article	IF	CITATIONS
91	Expression of Glut-1 in primary and recurrent head and neck squamous cell carcinomas, and compared with 2-[18F]fluoro-2-deoxy-D-glucose accumulation in positron emission tomography. British Journal of Oral and Maxillofacial Surgery, 2008, 46, 180-186.	0.4	33